24th COBEM - 2017

24th ABCM International Congress of Mechanical Engineering
December 3-8, 2017, Curitiba, PR, Brazil

# COBEM-2017-1707
# HYDRODYNAMIC ANALYSIS OF DEBRIS CONTAINMENT GRIDS IN HYDROPOWER PLANT USING POROUS MEDIA

**Eduardo Tadashi Katsuno**
**Felipe Santos de Castro**
**João Lucas Dozzi Dantas**
IPT - Institute for Technological Research, 532 Prof. Almeida Prado Ave., Cid. Universitária, Butantã, 05508-901, São Paulo/SP
katsuno@ipt.br
fscastro@ipt.br
jdantas@ipt.br

***Abstract.***
*Log booms are a type of debris containment grids developed specifically for containing logs. A log boom is an important part of Santo Antônio hydropower plant, retaining logs that are carried in the river, preventing damage to the turbine and maintains the energy generation. This paper aims to develop a simplified model of one log boom module using porous media. The main interest in simplification is at macro scale, especially in the module total force. With this development, it is expected to be possible to simulate a log boom line with accessible computational cost in future works. The hydrodynamic investigation is conducted using CFD software, in order to provide data for hydrodynamic analysis. This paper is divided in two main steps. Firstly, simulations of complete representation of log boom are performed. Next, a simplified model, using porous region and porous interface in specific parts to simplify the log boom geometry, is developed. The porosity coefficients are obtained through an iterative process to have forces similar to the complete model. It is observed that the porous region produced results close to the complete model, while the porous interface presented acceptable results for values of low advance velocities.*

***Keywords:*** *CFD, Porous media, Log boom, Hydropower plant*

## 1. INTRODUCTION

Debris containment grids are important part of hydropower plants, retaining large objects that can damage the turbines and reduce the power plant efficiency. In the case of the Madeira River, located in the Amazon rainforest in the north of Brazil the large amount of logs is the most significant debris related problem, reaching diameters of up to 2 m and lengths of 30 m. Log booms are a type of debris containment structures developed specifically for containing logs. The log booms developed by the Santo Antônio hydropower plant, located in the Madeira River, are presented in Fig. 1.

Figure 1. Log boom line in the Madeira river (left) and a log boom module (right)

A hydrodynamic analysis must be developed to provide data for a structural analysis, and thus, determine the critical load and develop structural improvements of log boom. However, a CFD simulation with the complete representation each log boom module is prohibited by computational cost, requiring to develop a simplified model.

## 2. OBJECTIVES

This paper aims to develop a simplified numerical model of one log boom module that are able to compute the hydrodynamic forces and moments generate by the grid and float part of the log boom with a low computation cost. On the future this model will be used to simulate several log boom modules, *i.e.* a log boom line, using 6 Degree of Freedom (DoF) to investigate how the line will behave. Therefore, the main interest in simplification is at macro scale, especially in the module total force. The hydrodynamic investigation is conducted using CFD software.

## 3. METHODOLOGY

In a later work in (Katsuno *et al.*, 2017), it was investigated the dynamic behavior and the hydrodynamic forces of a log Boom module in different flow velocity and direction, verifying the results by comparison to towing tank experiments (de Castro *et al.*, 2017). These results were used as a reference to the verify the accuracy of simplified model results. Therefore, this paper is divided in two parts. Firstly, were presented the results obtained by simulating a complete numerical model, *i.e.*, a model that represents most of the log boom details.Log boom was modeled as two linked bodies, floats and grid, using periodic condition to simulate the entire line. The link between bodies allow the assembly to move in the vertical direction, and the float unit, to rotate around the joint in the grid.

Next, a simplified model with considerably fewer elements was developed using porous approach in some parts to simplify the log boom structure into a simpler geometry. The porosity coefficients was the main concern in this step. The simplified model was simulated in the same operating conditions as the complete model. Then the forces in both bodies were compared and the porosity coefficients are updated to correct the differences. This process was repeated in an iterative way until the difference between forces on the models, *i.e.*, the residual, was reduced to acceptable value.

## 4. NUMERICAL MODELING

The software Siemens Star-CCM+ version 12.02.011, using double precision, was used for all CFD simulations. Water and air are considered incompressible and the unsteady Reynolds-averaged NavierâĂŞStokes (uRANS) equations are used to model the flow field. The Volume of Fluid (VoF) Eulerian multiphase model was used to represent interactions of both fluids. The flat wave model was used to define the multiphase conditions, using a numerical damping in inlet and outlet boundary conditions to minimize the effect of wave reflection and ensure a better convergence. The wave damping is done by adding a term of resistance in the z-momentum (coordinate in the direction of gravity) Navier-Stokes equations, following the method proposed by (Choi and Yoon, 2009).

Transient simulations, with an implicit unsteady approach, are used. At the beginning of simulations, the movements are frozen, due to the fluid stabilization. Then, the movements are gradually released and wait to stabilize. Finally, the time step is decreased, some more iterations are done and the results are collected.

The $k-\omega$ SST model, presented by (Menter *et al.*, 1994), is adopted. This model uses the traditional $k-\omega$ formulation near to the wall and $k-\epsilon$ formulation far from the wall, avoiding the high sensibility of $k-\omega$ model in the inlet regions of free-stream. The $k-\omega$ SST model is recommended instead of your traditional model (CD-Adapco, 2016).

## 5. SIMULATION OF COMPLETE REPRESENTATION

In this step, one log boom module is simulated for several velocities and side-slip angles. It is desired that there are two DoF of movement: rotation of the chassis and sinking of the assembly. This section is based on a previous paper of the same authors, available in (Katsuno *et al.*, 2017) and (de Castro *et al.*, 2017).

### 5.1 Domain Geometry and Boundary Conditions

The simulation of log boom line has a high computational cost. Therefore, just one module of log boom is simulated with the sides having a periodic condition. This simplification is valid once the log boom line is very large, having 100 to 200 times the modules length, and the angle between adjacent modules are very small, being possible to consider that the right side of a log boom module has the same flow field characteristics of the left side.

The rotation movement around the connection axis between grid and chassis is a DoF movement. To make it possible (using overset mesh, discussed in the next section), two regions are necessary: one that contains the domain and the grid and another that contains the chassis. The dimensions of each region are shown in Fig. 2.

The boundary conditions are presented in Fig. 3, showing the grid and the periodic interface. Note that the chassis region is covered by the overset boundary. This boundary allows an interpolation with another region, explained in the next section.

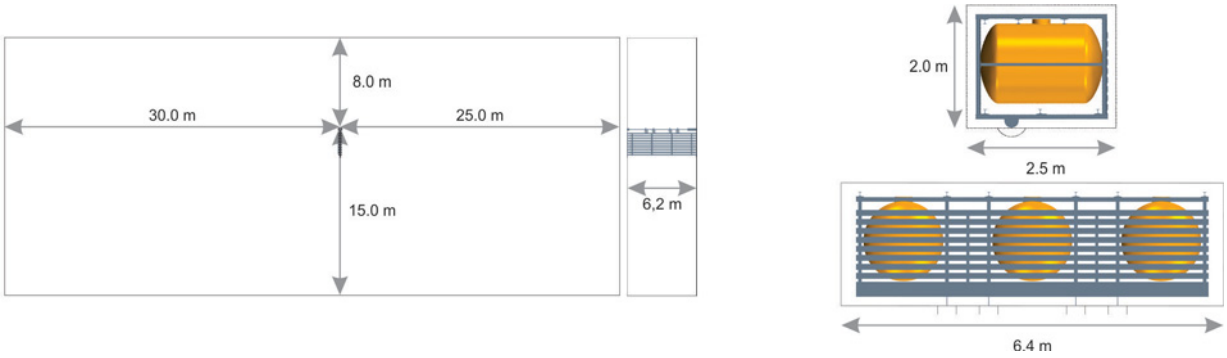


Figure 2. Geometric dimensions of domain (left) and chassis (right)

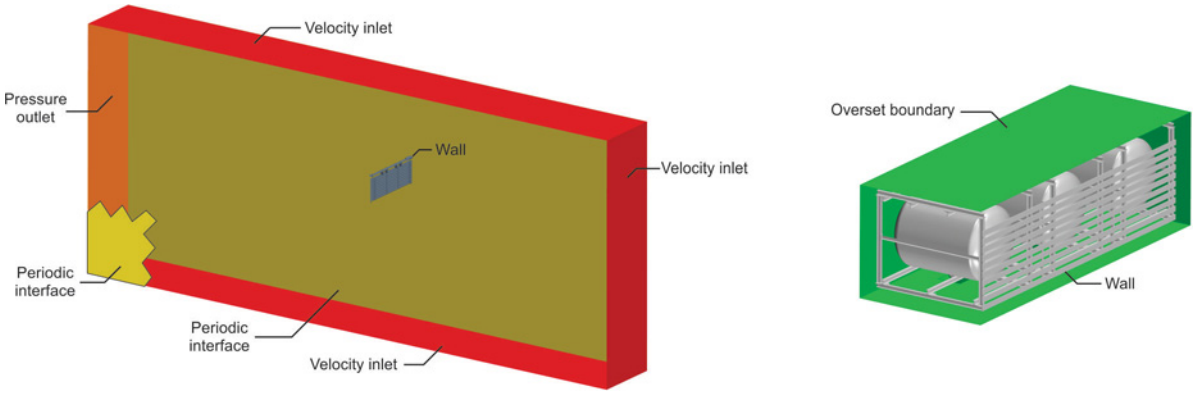


Figure 3. Boundary conditions of the domain (left) and chassis (right)

### 5.2 Mesh

In both regions, generating mesh using the trimmer topology (CD-Adapco, 2016) was used because of their good convergence and rapidity when compared to the polyhedral mesh, fact observed in previous simulations with propellers (Katsuno and Dantas, 2017).

In the domain region, volume controls for mesh refinement are made in regions close to the log boom, decreasing the density of elements according to the wake distance. Also, the elements are refined in water line region, for better representation of the wave. An important volume control is that allows the chassis region to rotate, once it maintains the elements inside with the same dimensions of the chassis mesh. The refining volumes and domain mesh are presented in Fig. 4.

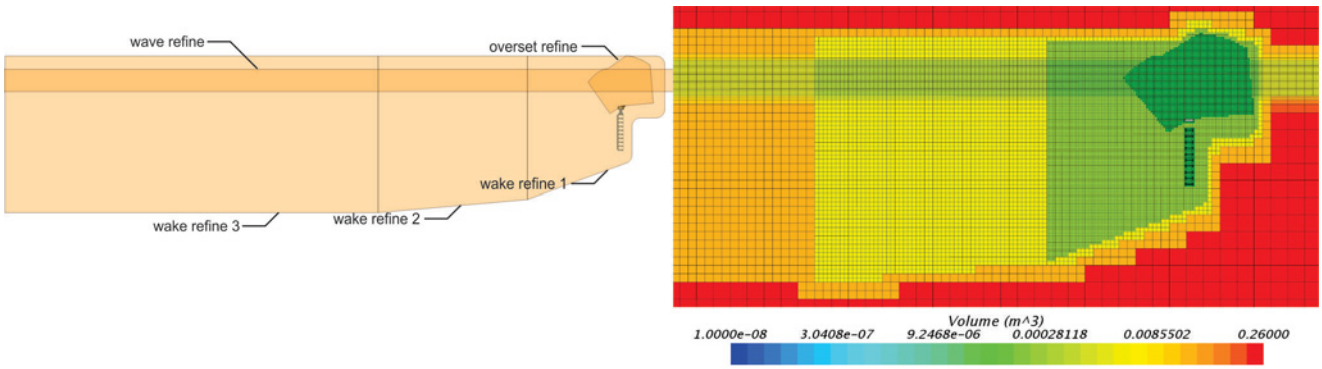


Figure 4. Refining volumes (left) and mesh (right) of domain region

Figure 5 (left) shows the chassis mesh. As can be noted, the elements, especially at the edges, have dimensions similar to the domain mesh inside the overset refine volume. This is a requirement to interpolate the two meshes in order to generate a unified resulting mesh, as schematized in Fig. 5. In the figure, before the interpolation, it can seen two overlapping meshes (chassis mesh in red and the domain mesh in light-yellow). After interpolation, it is considered that regions outside the chassis use the domain mesh; overlap regions use the chassis mesh; and at the edge there is an intermediate cell zone.

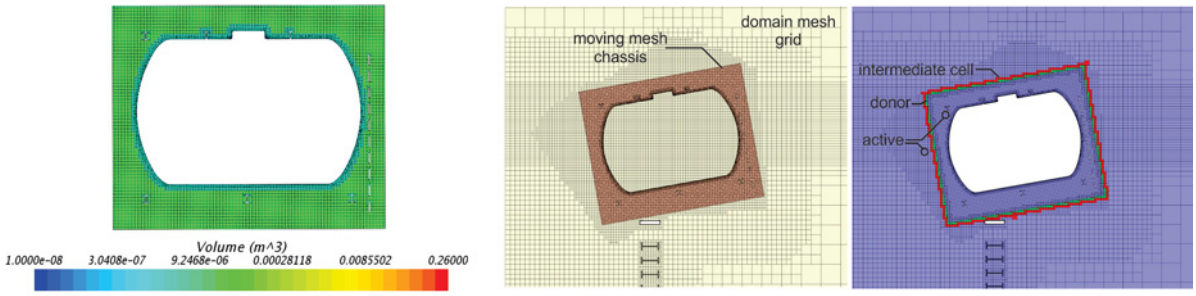


Figure 5. Mesh of chassis (left) and overset schema (right)

The edge between these two meshes has an intermediate zone, belonging to two regions. If the element size of one mesh is too coarse compared to another mesh, the interpolation element is insufficient and cannot be done. It is recommended to have, in the edge zone, 4-5 elements of each mesh, according to (CD-Adapco, 2016). Note that the range of rotation is limited by the overset refine. An essential advantage of this method is that the mesh is interpolated at each time-step, allowing rotation of the chassis region without spending time remeshing.

### 5.3 DFBI - Dynamic Fluid Body Interaction

There are two DoF: sinkage of the entire module and rotation between grid and chassis. To allow the rotation, the overset approach is used, as explained before. For the sinkage movement, there was no need to use an overset approach, once the wave line reference can change along the boundaries. A schematic of sinkage and rotation are represented in Fig. 6.

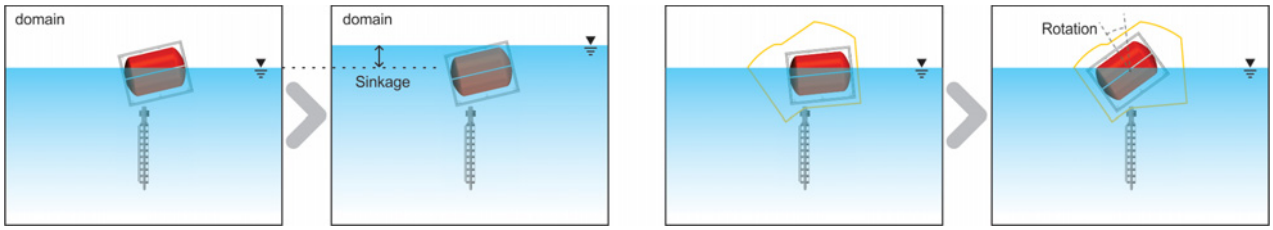


Figure 6. Two DoF: Sinkage (left) and Rotation (right)

### 5.4 Results

Simulations with five advance velocities and seven side-slip angles are done. Figure 7 schematizes the side-slipe angle $\beta$ and advance velocity $v_a$, input parameters of the simulations. The result of rotation and sinkage ( distance of the rotation axis to the water line) were presented in Fig.8. The longitudinal and lateral forces (relative to the log boom coordinate system) are shown in Fig.9.

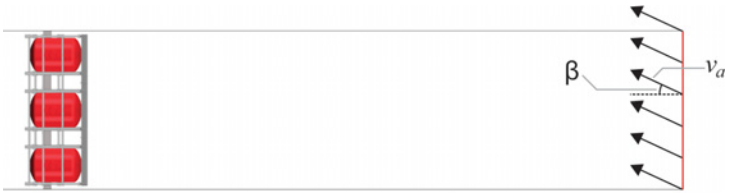


Figure 7. Top view. Advance Velocity ($v_a$) and side-slip angle ($\beta$) of velocity inlet

## 6. SIMULATION WITH SIMPLIFIED REPRESENTATION

To allow the comparison between complete and simplified model, the same conditions of the complete model were used, whenever feasible. It is desired to use a porous media to simplify the geometry of grid and the metallic structure of the chassis.

The porous media can be simulated using two approaches: porous interface and porous region. The porous interface consists of a baffle surface that allows the passage of fluid with a pressure drop. Because it is a surface, it does not have volume and its drag force due to pressure drop is computed only in the surface normals, not having a lateral components.

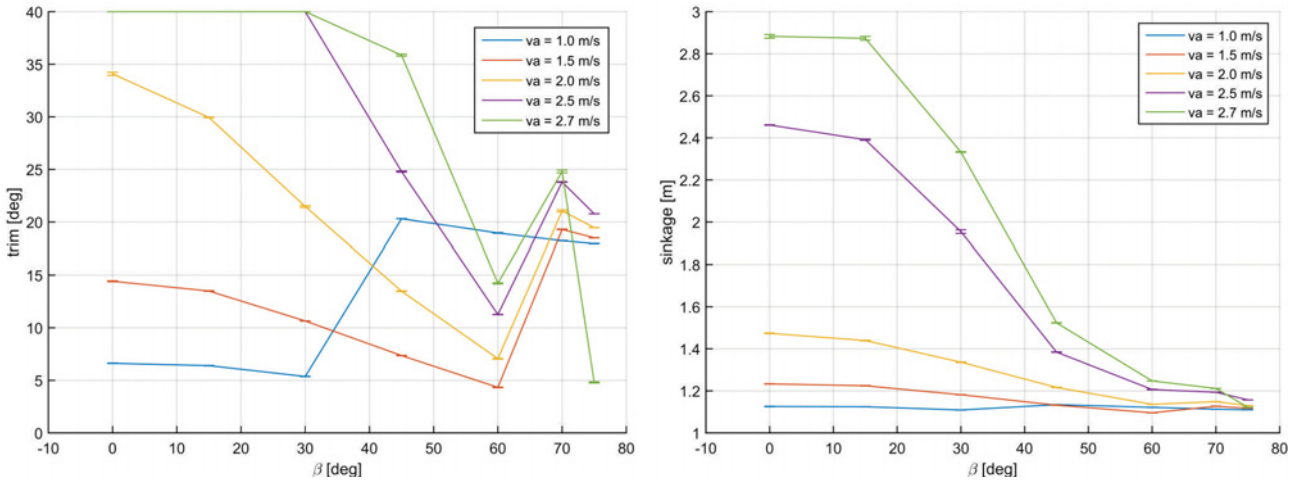


Figure 8. Trim angle of the chassis (left) and sinkage (right)

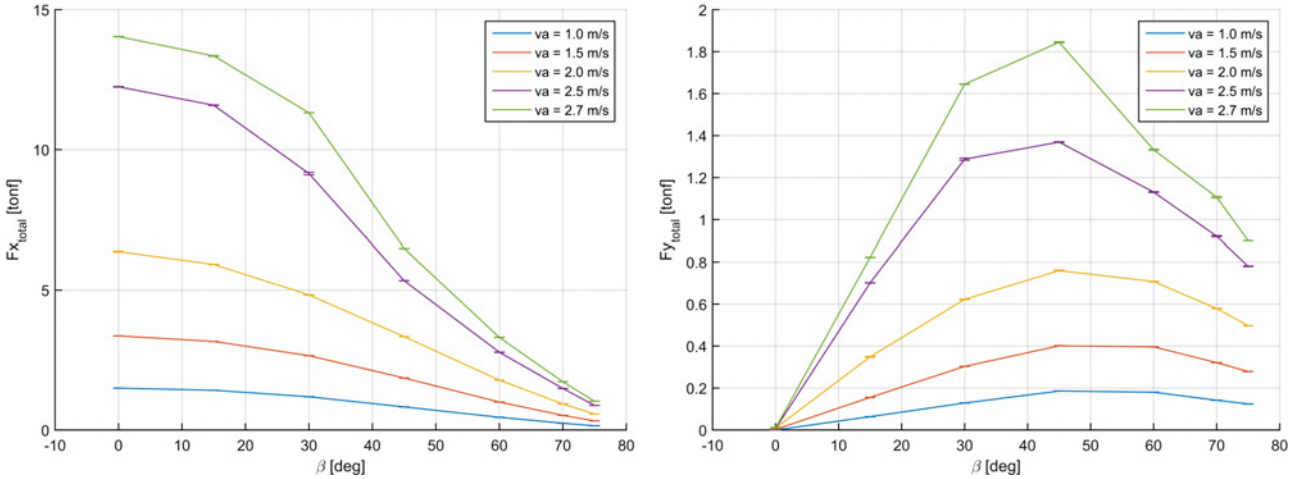


Figure 9. Frontal force (left) and lateral force (right), in tonne-force

The porous region, however, deals with a volume in which it allows the passage of fluid. In this type, because it is a three-dimensional region, a different pressure loss can be imposed for each direction of the flow, being able to have different quantities of forces in each coordinate.

The porous interface was used in the frontal part of chassis. This modeling was chosen because the front of chassis has a thinner structure compared to grid and the lateral force is given by the drag of floats. In the case of the grid, the force compositions were made only by the porous region, once there are no other walls. In this case, a porous region is necessary in order to artificially generate lateral forces.

To maintain the same sinkage and rotation of the previous model and reduce the computation cost, DFBI was not used in this type of simulation. Sinkage and rotation values are obtained from the complete model and maintained stationary.

### 6.1 Domain Geometry and Boundary Conditions

The domain dimensions were the same as the complete representation, to allow comparison in the same conditions. The grid was represented by a porous region and the front of the chassis, by a porous interface. To allow this, a grid-exclusive region is required.

Figure 10 shows the boundary conditions of three regions used. The domain region, in this case, has a hole in which its surface is connected to the grid region, through a internal interface. As domain region, there are a periodic interfaces at sides.

The chassis region is composed of a box with empty space and another box, with same dimensions as the empty space space. The smaller box represents the chassis, with one face with porous interface. In Fig. 10 (III), this box can be observed through the internal interface and porous baffle surfaces.

The larger box is needed for an overset interface, as well as simulations of the complete model. Although it does not require strictly an overset interface, since this simulation type does not uses DFBI, it was decided to use for not requiring remeshing in each simulation condition, using the same base mesh.

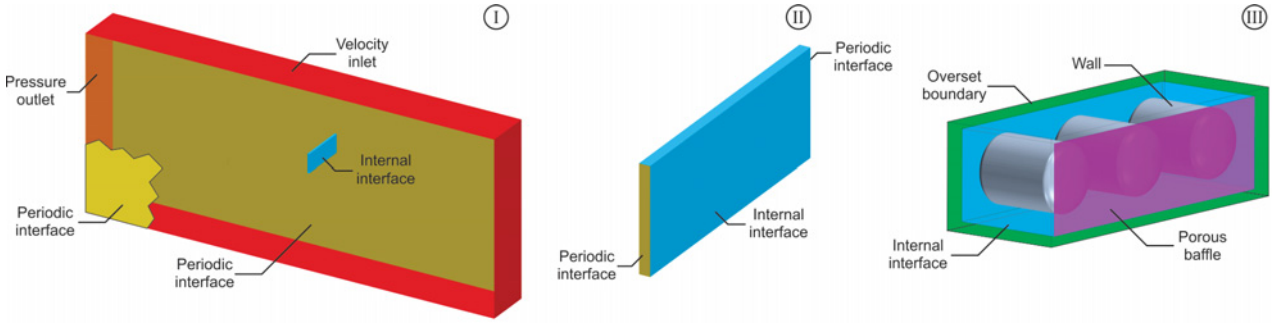


Figure 10. Boundary Conditions of Domain (I), Grid (II) and Chassis (III) regions (figures are not in the same scale)

### 6.2 Mesh

The mesh has the same refining volumes as the complete model, described in Sec. 5.2, but with a larger element size specified to the refinement. Figure 11 shows the size of the elements in each region.

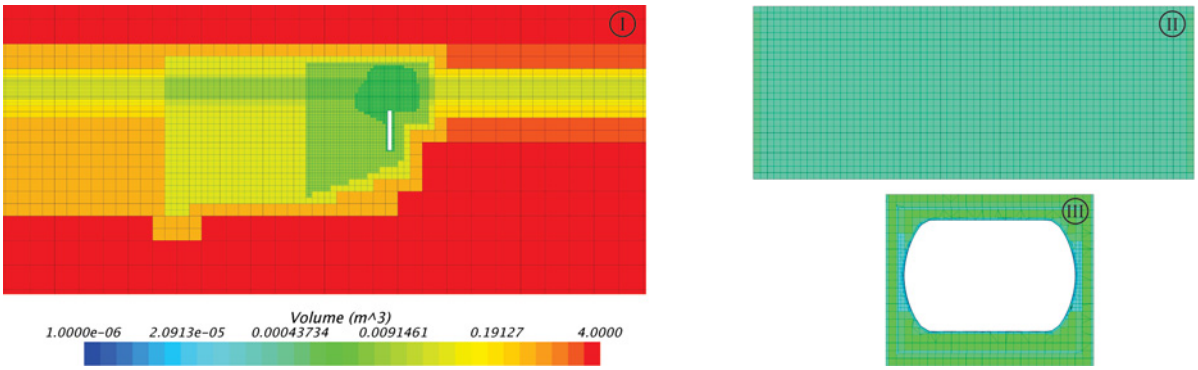


Figure 11. Mesh of Domain (I), Grid (II) an d Chassis (III) regions (figures are not in the same scale).

Note that the number of elements is smaller than the complete model, to save computational cost. As a comparative, Tab. 1 shows the number of elements and faces between the complete and simplified model. Note that in the complete model, the grid and domain consist in the same region.

Table 1. Comparative number of elements and faces.

| | Elements (Cells) | | Interior Faces | |
|---|---|---|---|---|
| | Complete | Simplified | Complete | Simplified |
| Chassis | 2 209.7 k | 58.5 k | 6 622.1 k | 162.2 k |
| Domain | 1 857.3 k | 153.2 k | 5 461.5 k | 460.1 k |
| Grid | | 6.8 k | | 18.5 k |
| Total (without overset interpolation) | 4 067.0 k | 218.5 k | 12 083.6 k | 640.8 k |

### 6.3 Porous Modeling

The modeling inside a porous region is based on superficial velocity. The continuity and momentum equations are given by Eq. (1) and Eq. (2), respectively.

$$\frac{\partial}{\partial t}\int_{\Omega}\rho\frac{V_f}{V}dV+\oint_{\partial\Omega}\rho\mathbf{v_s}\cdot d\mathbf{a}=0 \tag{1}$$

$$\frac{\partial}{\partial t}\int_{\Omega}\rho\mathbf{v_s}dV+\oint_{\partial\Omega}\rho\mathbf{v_s}\otimes\mathbf{v_s}\cdot d\mathbf{a}=\oint_{\partial\Omega}p\mathbf{I}\cdot d\mathbf{a}+\oint_{\partial\Omega}\mathbf{T}\cdot d\mathbf{a}+\int_{\Omega}\mathbf{f_b}dV+\int_{\Omega}\mathbf{f_p}dV \tag{2}$$

In Eq. (1) and Eq. (2), $V_f$ is the volume occupied by the fluid; $V$, total volume of porous region; $\rho$, fluid density; and $\mathbf{v_s}$, the superficial velocity, given by Eq. (3).

$$\mathbf{v_s} = \frac{V_f}{V}\mathbf{v} \tag{3}$$

In Eq. (2), $\otimes$ is the Kronecker product; $p$, pressure; $\mathbf{T}$, viscous stress tensor; $\mathbf{f_b}$, resultant of body forces per volume; and $\mathbf{f_p}$, the porous medium resistance force per volume, given by Eq. (4).

$$\mathbf{f_p} = -\left(\mathbf{P}_\nu + \mathbf{P_i}\left|\mathbf{v_s}\right|\right)\cdot\mathbf{v_s} \tag{4}$$

In Eq. (4), $\mathbf{P}_\nu$ and $\mathbf{P_i}$ are the viscous and inertial resistance tensor.
For the porous interface, the pressure drop $\Delta p$ is given by the Eq. (5).

$$\Delta p = -\rho\left(\alpha_i\left|\mathbf{v_s}\cdot\mathbf{n}\right| + \alpha_\nu\right)\mathbf{v_s}\cdot\mathbf{n} \tag{5}$$

In Eq. (5), $\mathbf{n}$ is the normal vector of the porous surface; $\alpha_i$ and $\alpha_\nu$, porous inertial and viscous resistance.

### 6.4 Obtaining porosity coefficients

The porosity coefficients can be defined in such that the forces results in values close to those obtained in the complete representation model. The porosity tensors $\mathbf{P}_\nu$ and $\mathbf{P_i}$ have all components related to the $z$-coordinate equal to zero because, as seen in previous sections, there are no vertical components of advance velocity. Therefore, $\mathbf{P}_\nu$ and $\mathbf{P_i}$ are given by Eq. (6).

$$\mathbf{P}_\nu = \begin{bmatrix} p_{\nu xx} & p_{\nu xy} & 0 \\ 0 & p_{\nu yy} & 0 \\ 0 & 0 & 0 \end{bmatrix} \quad ; \quad \mathbf{P_i} = \begin{bmatrix} p_{ixx} & p_{ixy} & 0 \\ 0 & p_{iyy} & 0 \\ 0 & 0 & 0 \end{bmatrix} \tag{6}$$

To obtain the coefficients, an iterative method is used that compares the result obtained by the simplified model with the result of complete model and was considered as a residual that needs to be minimized in the next iteration. Figure (12) shows schematically the process of obtaining these coefficients. Each step is explained in detail below.

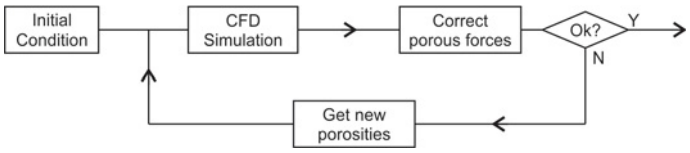


Figure 12. Flowchart method of the iterative method to determine the porosity coefficients

**Initial condition** Obtaining the initial guess of porosity coefficients is such that it satisfy the linear equation given in Eq. (7).

$$f_{c\bullet} = \mathbf{v}_p \cdot \mathbf{p_{i\nu}} \tag{7}$$

Each term of Eq. (7) varies between the grid x-coordinate, grid y-coordinate and the frontal grid of chassis, given respectively by Eq. (8), Eq. (9) and Eq. (10).

$$\text{grid x-coordinate}: \begin{cases} \mathbf{v_p} = \dfrac{V_f}{V}\left[v_a\cos\beta\left|v_a\cos\beta\right| \quad v_a\sin\beta\left|v_a\sin\beta\right| \quad v_a\cos\beta \quad v_a\sin\beta\right]^T \\ \mathbf{p_{i\nu}} = \left[p_{ixx} \quad p_{ixy} \quad p_{\nu xx} \quad p_{\nu xy}\right]^T \\ f_{c\bullet} = \dfrac{f_{cx}}{V} \end{cases} \tag{8}$$

$$\text{grid y-coordinate}: \begin{cases} \mathbf{v_p} = \dfrac{V_f}{V}\left[v_a\sin\beta\left|v_a\sin\beta\right| \quad v_a\sin\beta\right]^T \\ \mathbf{p_{i\nu}} = \left[p_{iyy} \quad p_{\nu yy}\right]^T \\ f_{c\bullet} = \dfrac{f_{cy}}{V} \end{cases} \tag{9}$$

$$\text{frontal grid of chassis :} \begin{cases} \mathbf{v_p} = \dfrac{V_f}{V}\begin{bmatrix} v_a\cos\beta & |v_a\cos\beta| & v_a\cos\beta \end{bmatrix}^T \\ \mathbf{p_{i\nu}} = \begin{bmatrix} \alpha_i & \alpha_\nu \end{bmatrix}^T \\ f_{c\bullet} = \dfrac{f_{gx}}{\rho S_g} \end{cases} \tag{10}$$

In Eq. (8), Eq. (9) and Eq. (10), $v_a$ is the advance velocity; $S_g$, the area of porous baffle; $f_{cx}$, force x-direction of grid in the complete model simulation;$f_{cy}$, force y-direction of grid in the complete model simulation and; $f_{gx}$, force x-component of the frontal grid of chassis in the complete model simulation.

It is expected that the results do not give exactly the values of the complete model since it is assumed that the velocity inside the porous region or normal to porous surface are the same as the advance velocity, in far field, *i.e.*, it is considered that the portion of induced velocity , as a first guess, is zero.

There were 35 simulations, combination of 5 advance velocities and 7 side-slip angles, and it must obtain the porosity coefficients that best fit all of these cases. Therefore, a Linear Least Squares approach is used in which it must satisfy the minimization problem described in Eq. (11).

$$\begin{aligned} &\underset{\mathbf{p_{i\nu}}}{\textbf{Min}} && \frac{1}{2}\|[\mathbf{v_p}]\cdot\mathbf{p_{i\nu}} - [f_{c\bullet}]\|_2^2 \\ &\text{such that} && \mathbf{p_{i\nu}} \geq 0 \end{aligned} \tag{11}$$

In Eq. (11), $[\mathbf{v_p}]$ and $[f_{c\bullet}]$ are matrices formed by all 35 simulations. For example, in the case of grid x-coordinate, $[\mathbf{v_p}]$ has dimensions of $35 \times 4$.

**CFD Simulation** Simulation were performed with porosity information as input and the output are divided in components of surface-integral and volume-integral forces, as shown schematically in Eq. (12). This separation is done because the porosity affects explicitly only the volume-integral term of force.

$$\text{sim}\left(\mathbf{p_{i\nu}}^{[i]}\right) = f_{\partial\Omega}^{[i]} + f_{\Omega}^{[i]} \tag{12}$$

Based on the Eq. (2), $f_{\partial\Omega}$ and $f_\Omega$ can be defined as Eq. (13) and Eq. (14).

$$f_{\partial\Omega} = \oint_{\partial\Omega} p\mathbf{I}\cdot d\mathbf{a} + \oint_{\partial\Omega} \mathbf{T}\cdot d\mathbf{a} \tag{13}$$

$$f_\Omega = \int_\Omega \mathbf{f_p} dV \tag{14}$$

As the body forces are composed only by weight and gravity has terms only in the z-direction, this force does not appear in Eq. (14).

**Correct the porous forces** It is expected that the error obtained in the simulation is due to an incorrect value in the velocity. Therefore, each term of the velocity is multiplied by a correction factor $\mathbf{k}$ in order to fit to the force due to porous medium, as shown in Eq.( 15).

$$f_\Omega^{[i]} = \mathbf{p_{i\nu}}^{[i]} \circ \mathbf{v_p}\cdot\mathbf{k}^{[i]} \tag{15}$$

where $\circ$ is the Hadamard product (element-wise product of two matrix with same dimensions). Linear Least Squares approach is made between all conditions in order to obtain the correction $\mathbf{k}$ that best fits all the results obtained.

**Get new porosities** With the correction factor $\mathbf{k}$ , a linear system is made for determinate the porosity to obtain the desired force. Since the total force of a porous region is composed of the surface-integral and volume-integral forces, the term of surface must be discounted due to obtain only the volume-integral force term, as shown in Eq.( 16).

$$f_{c\bullet} - f_{\partial\Omega}^{[i]} = \mathbf{v_p} \circ \mathbf{k}^{[i]} \cdot \mathbf{p_{i\nu}}^{[i+1]} \tag{16}$$

Again, Linear Least Squares approach is used to obtain the next iteration of porosity coefficients, $\mathbf{p_{i\nu}}^{[i+1]}$.

### 6.5 Results

Figure 13 shows the comparison between the force magnitude obtained with the complete model simulation (in solid line) and the result after 6 iterations of the simplified simulation result using the porosity media (in dashed line) for several advance velocity. In the same figure, it show the results of force x-direction of the front grid of chassis for complete and porous model.

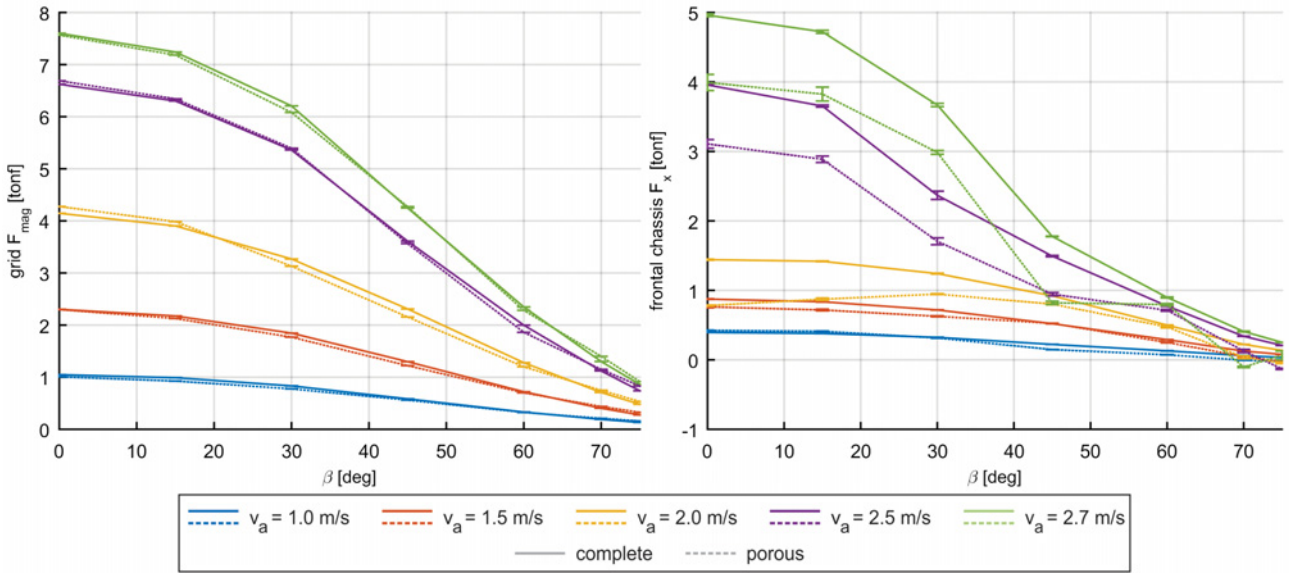


Figure 13. Comparative of complete and porous model in grid force (left) and frontal chassis force (right)

Figure 14 shows the convergence of porous model along the iterations. In both cases, there are good convergences, with descending values. Observing for the case of the porous region, 4 iterations would already have satisfactory results. For the front chassis model, there is a downward trend for more iterations.

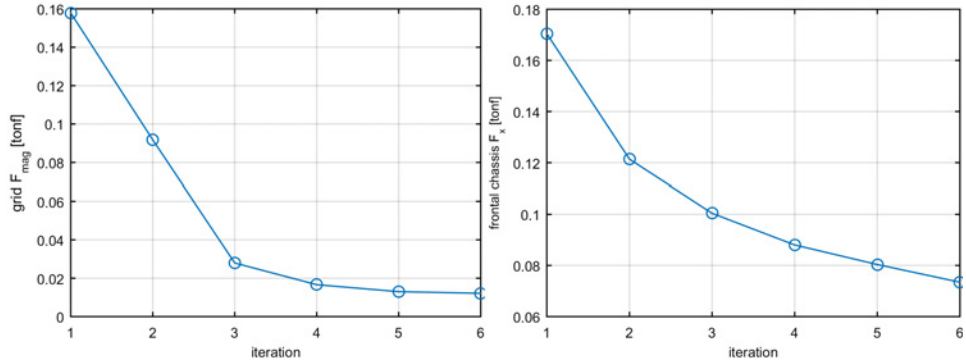


Figure 14. Mean $\ell^2$-norm (Euclidean norm) evolution

It can be observed that the porous model results in values close compared to the complete model, satisfying the requests. However, the surface interface model used for the front chassis presented less satisfactory results, specially for high values of advance velocities. Figure 15 shows a comparison with the VOF scalar. It can be noted that the coarse mesh used in simplified model was insufficient to model all the details of the free surface

Fig. 16 shows a comparison in velocity. The porosity coefficients are constant along the grid and, becase of this, it can not be noted the the generation of vortices as in the complete model. However, as the main concern is on macro scales forces, it is expected that both the difference observed in the VOF and in the generation of vorticity are not significant for the simulation of the log boom line.

## 7. CONCLUSIONS

The objectives using the porous approach were satisfactorily achieved, since the simulation time was noticeably lower. The results with porous region, used to simplify the grid, had results almost identical to those obtained with the complete model. However, for the porous interface, used to simplify the front chassis, the simulation results achieved different values, specially for higher advance velocities.

Figure 15. Comparative of VOF between complete (left) and simplified (right) model - $v_a = 2.0$ m/s and $\beta = 0$ deg

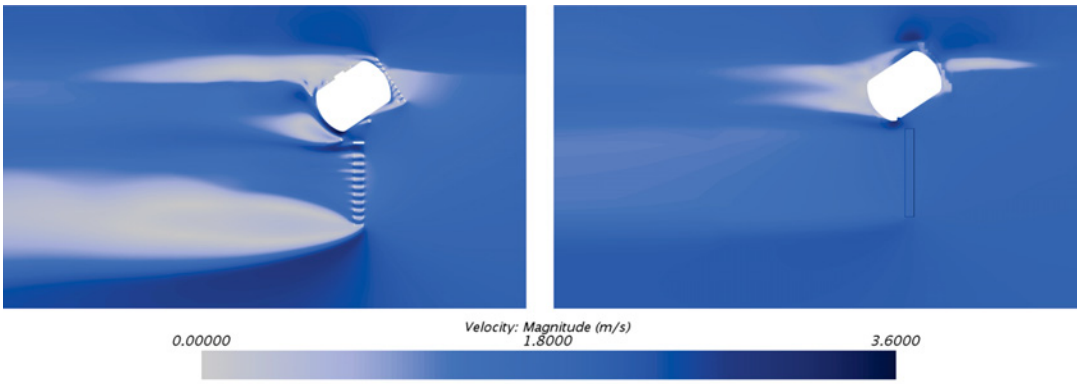


Figure 16. Comparative of Velocity (magnitude) between complete (left) and simplified (right) model - $v_a = 2.0$ m/s and $\beta = 0$ deg

For future work, it is intended to implement the porous volume also for the chassis region to check if the results are as close as the grid results. With the porosity coefficients defined in this work, a DFBI model will be implemented, similar to the complete model, with degrees of freedom of sinking and rotation, and it will be verified if it porous model simulation reaches the same equilibrium point as complete model simulation. In a satisfactory case, a line of log booms formed by several log booms connected by rotational joints will be simulated with an accessible computational cost.

## 8. ACKNOWLEDGMENTS

The authors would like to thank the laboratory technicians for conducting the tests, the Fundação de Apoio ao Instituto de Pesquisas Tecnológicas (FIPT), the Santo Antônio Energia for funding the project, through the Research and Development fund (PD-06683-0116/2016) of Brazilian Electricity Regulatory Agency (in Portuguese, Agência Nacional de Energia Elétrica, ANEEL).

## 9. REFERENCES

CD-Adapco, 2016. *Star-CCM+ v.11.02 User Guide*, latest edition.

Choi, J. and Yoon, S.B., 2009. "Numerical simulations using momentum source wave-maker applied to rans equation model". *Coastal Engineering*, Vol. 56, No. 10, pp. 1043–1060.

de Castro, F.S., Katsuno, E.T. and Dantas, J.L.D., 2017. "Instrumentation methodology for a log containment grid model in towing tank tests". In *The 30th American Towing Tank Conference*. The Society of Naval Architects and Marine Engineers.

Katsuno, E.T. and Dantas, J.L.D., 2017. "Analysis of the blockage effect on a cavitation tunnel using cfd tools". In *ASME 2017 36th International Conference on Ocean, Offshore and Arctic Engineering*. American Society of Mechanical Engineers, pp. V07BT06A043–V07BT06A043.

Katsuno, E.T., de Castro, F.S. and Dantas, J.L.D., 2017. "Debris containment grid cfd validation with towing tank tests". In *The 30th American Towing Tank Conference*. The Society of Naval Architects and Marine Engineers.

Menter, F.R. *et al.*, 1994. "Two-equation eddy-viscosity turbulence models for engineering applications". *AIAA journal*, Vol. 32, No. 8, pp. 1598–1605.

## 10. RESPONSIBILITY NOTICE

The authors are the only responsible for the printed material included in this paper.